AIAA JOURNAL
Vol. 45, No. 8, August 2007

Failure of Dynamically Loaded Thermoelastoviscoplastic Rectangular Plate

R. C. Batra*
Virginia Polytechnic Institute and State University, Blacksburg, Virginia 24061
and
S. Romano†
Bensalem, Pennsylvania 19020

DOI: 10.2514/1.28155

The initiation and propagation of a crack and an adiabatic shear band in three-dimensional finite coupled thermomechanical deformations of a homogeneous and isotropic thermoelastoviscoplastic rectangular 4340 steel plate containing a centrally located through-the-thickness elliptic void and deformed in simple tension are analyzed numerically by using the finite element computer code DYNA3D. Initially, the major and the minor axes of the elliptic void coincide with the centroidal axes of the plate. An element is assumed to have failed when the damage parameter defined in terms of histories of the effective plastic strain, the effective plastic strain rate, the triaxiality factor, and the temperature at its centroid equals one; an adiabatic shear band initiates at a point when the effective plastic strain there equals one, while the material point is deforming plastically and deformations of the surrounding material are inhomogeneous. It is found that the ratio R of lengths of the two principal axes of the void significantly influences when and where a crack and an adiabatic shear band initiate and which one initiates first. They usually originate from a point on the surface of the elliptic void which is also on the midsurface of the plate, and they propagate faster in the thickness direction. An adiabatic shear band initiates sooner in the three-dimensional simulations than when displacements in the thickness direction are constrained to vanish. The crack tip follows a zigzag path that does not lie in one plane.

I. Introduction

FAILURE of structures under dynamic loads is of considerable interest because of severe damage caused to them by blast/shock loads, hurricanes, fire, and earthquakes. Usually, dynamic failure of ductile materials is preceded by the initiation and the development of adiabatic shear bands (ASBs) which are narrow regions, a few micrometers wide, of intense plastic deformation with plastic strains of about 100%. Even though heat conduction plays a significant role in determining their widths, they are called adiabatic because there is not enough time for the heat to be conducted away. Tresca [1] observed them over a century ago during the hot forging of a platinum bar; subsequently, they were also reported by Massey [2]. However, activity in the field picked up after Zener and Hollomon [3] observed them during the punching of a hole in a low carbon steel plate. Analytical works (e.g., see Clifton [4]) have assumed that an adiabatic shear band initiates when the shear stress in a simple shearing problem or the effective stress in a three-dimensional problem attains its maximum value. Bai's [5] analysis of infinitesimal perturbations superimposed on finite homogeneous deformations also gives the same result. Numerical solutions of nonlinear coupled equations governing simple shearing and plane-strain thermomechanical deformations of a thermoelastoviscoplastic body reveal that an ASB forms much later than when the effective stress attains its maximum value [6,7]. Much of the work done on ASBs is summarized in two books [8,9]. Recently, the initiation and growth of ASBs have been studied in "hat-type" specimens by Bronkhorst et al. [10] by assuming the deformations to be axisymmetric. They used the mechanical threshold stress (MTS) constitutive relation, Gurson's [11] flow surface, and the commercial finite element (FE) code EPIC. Adiabatic shear banding in axisymmetric deformations has also been studied by Batra and Ko [12] who adaptively refined the FE mesh to delineate the width of an ASB.

Analyses of two- and three-dimensional deformations of a prenotched plate impacted on the notched side have revealed that under otherwise identical conditions, the failure initiates sooner in the three-dimensional analysis than in the two-dimensional analysis [13,14]. Also, the failure usually ensues from a point inside the three-dimensional structure which cannot be predicted by the two-dimensional analysis, and easily delineated through experiments because experimental observations are generally made on the bounding surfaces of a body. Besides values of material parameters, loading conditions, and the shape of the body, the time of failure initiation and from where it originates also strongly depend upon the number, the type, and the distribution of defects in the body. Here, to simplify the problem, we investigate crack/ASB initiation from a through-the-thickness elliptic void in an otherwise homogeneous rectangular plate loaded in simple tension. Variables which affect the initiation and the development of ASBs and cracks include material parameters (mass density, specific heat, thermal conductivity, strain hardening, thermal softening, strain-rate hardening), state of deformation (the maximum shear stress, maximum shear strain, maximum shear strain rate, temperature rise, hydrostatic pressure, and triaxiality factor), the microstructure (size, shape, spacing, orientation, population, and distribution of second phase particles, inclusions, precipitates, etc., as well as texture, porosity, imperfections, and thermal stability of microstructures), and external loading conditions (disturbances and discontinuities imposed externally, their amplitude, sharpness, distributions, and energy). It is impossible to characterize the effect of each individual parameter because it interacts with other parameters in a rather complicated way.

Even though an ASB separates two zones of widely varying strains, there is no decohesion and no free surface created. The

Received 3 October 2006; accepted for publication 6 March 2007.

*Dedicated to survivors of the 16 April 2007 tragedy in Norris Hall, Virginia Tech.

Department of Engineering Science and Mechanics, M/C 0219; rbatra@vt.edu.

†526 Beacons Court, Apartment C-1.

deformed body remains intact and continuous with thin layers of large gradients of shear strain in them. An ASB generally precedes ductile fracture. In fact, the fracture induced by ASBs might be due to the accumulation of microscopic damage in it because of the large plastic deformations and the consequent temperature rise.

The ASBs are sometimes desirable. For example, in the penetration of depleted uranium kinetic energy rods into steel targets, ASBs continuously sharpen the penetrator nose resulting in a deeper tunnel in the target. They also facilitate the punching of a hole in a metal cutting process because the kinetic energy required to perforate a centimeter thick plate by plugging equals nearly that needed to indent the same plate by less than 1 mm.

Most of the previous analyses of ASBs have considered either one- or two-dimensional problems. Except for Batra and Wang [14], other authors [13,15,16] used the computer code DYNA3D to analyze three-dimensional ASB problems. We note that in DYNA3D the problem formulation assumes locally adiabatic deformations, i.e., effects of heat conduction are neglected. Thus, the ASB width cannot be ascertained. However, the rise in the temperature of a material point due to the plastic dissipation is computed, and its influence on the yield stress considered. It has been shown that thermal conductivity does not influence the ASB initiation time much but significantly affects the post-ASB deformations, and the bandwidth [17,18]. Here, we use DYNA3D to study coupled thermomechanical deformations of a rectangular plate containing a through-the-thickness elliptic void and deformed in simple tension with the goal of delineating whether an ASB or a crack ensues first. The possibility of a crack initiating from the tip of an ASB or vice versa is not ruled out. As one may expect, computed results depend upon the ASB and the crack initiation criteria which for three-dimensional coupled thermomechanical high-strain-rate deformations are not available because of a lack of test data. As far as we can ascertain, the possibility of a crack and/or an ASB initiating simultaneously or sequentially has not been thoroughly examined. In the analysis of a plane-strain problem, Batra and Love [19] assumed that either an ASB or a crack but not both may originate. The thermomechanical properties of the material of the body, loading conditions, defects in the body, and the initiation criteria determine whether an ASB or a crack, or both, or multiple ASBs or several cracks ensue from one or more points in the body.

The rest of the paper is organized as follows. Section II gives formulation of the problem including the ASB and the crack initiation criteria and the simulation of the crack propagation. Section III discusses results, and Sec. IV summarizes conclusions.

II. Formulation of the Problem

A. Governing Equations

A schematic sketch of the problem studied is shown in Fig. 1. A rectangular SAE 4340 steel plate with an elliptic void through the plate thickness is pulled in the vertical direction by an axial velocity $V(t)$, prescribed on the top and the bottom surfaces that increases linearly from zero to its steady-state value in 1 μs. We use the referential or the Lagrangian description of motion and the rectangular Cartesian coordinates, with the origin at the centroid of the plate's back surface, to describe dynamic locally adiabatic thermomechanical deformations of the plate assumed to be made of an isotropic and homogeneous thermoelastoviscoplastic material that exhibits strain- and strain-rate hardening and thermal softening. These are characterized by the Johnson–Cook [20] relation

$$\sigma_y = [A + B(\varepsilon^p)^n]\left(1 + C\,\ell n\,\frac{\dot{\varepsilon}^p}{\dot{\varepsilon}_0}\right)(1 - \mathrm{T}^{*m}) \tag{1}$$

in which the flow stress σ_y increases with an increase in the effective plastic strain ε^p, the effective plastic strain rate $\dot{\varepsilon}^p$, but decreases with an increase in the temperature T of a material particle $T^* = (T - T_0)/(T_m - T_0)$; T_m is the presumed melting temperature of the material and T_0 is the initial temperature. Usually, T_m is determined by fitting curves to the test data; thus, it need not equal the actual melting temperature of the material. In Eq. (1), parameters B and n characterize the strain hardening of the material, C and $\dot{\varepsilon}_0$ its strain-rate hardening, and T_m and m its thermal softening.

Deformations of the plate are governed by the balance of mass, linear momentum, moment of momentum, and internal energy, which may be found in a continuum mechanics book (e.g., see Truesdell and Noll [21], Batra [22]).

We assume that the plate is initially at rest, at a uniform temperature, and is stress free. Because of the symmetry of the plate geometry, initial conditions, and the applied load, we assume that deformations are symmetric about planes $x_1 = X_1 = 0$, $x_2 = X_2 = 0$, and $x_3 = X_3 = 0.02H$. Thus, deformations of only one-eighth of the body occupying the region $0 \le X_1 \le H, 0 \le X_2 \le H, 0.02H \le X_3 \le 0.04H$ are analyzed. Boundary conditions (2b) and (2c), and (2e), listed next, arising from the symmetry of deformations, are imposed at points on the centroidal planes $X_1 = 0$, $X_2 = 0$, and $X_3 = 0.02H$. The vertical surface $X_1 = H$ is taken to be traction free and thermally insulated; see Eq. (2a). Normal velocity, null tangential tractions, and zero heat flux are prescribed on the top horizontal surface $X_2 = H$; these are given by Eq. (2d). In Eq. (2d), $t_0 = 1$ μs. The surface $X_3 = 0.04H$ is taken to be traction free and thermally insulated, and the surface $X_3 = 0.02H$ free of tangential tractions and constrained from moving in the X_3 direction; see Eq. (2e) and Eq. (2f). As implied by Eqs. (2a)–(2g), the surface of the elliptic void is taken to be traction free and thermally insulated.

$$T_{31} = T_{21} = T_{11} = 0, \quad Q_1 = 0 \qquad \text{on } X_1 = H \tag{2a}$$

$$T_{31} = T_{21} = 0, \qquad v_1 = 0, \qquad Q_1 = 0 \qquad \text{on } X_1 = 0 \tag{2b}$$

$$T_{32} = T_{12} = 0, \qquad v_2 = 0, \qquad Q_2 = 0 \qquad \text{on } X_2 = 0 \tag{2c}$$

$$T_{32} = T_{12} = 0, \qquad Q_2 = 0, \qquad v_2 = \begin{cases} \frac{v_0}{t_0}t, & 0 \le t \le 1\ \mu\text{s} \\ v_0, & t \ge 1\ \mu\text{s} \end{cases} \quad \text{on } X_2 = H \tag{2d}$$

$$T_{13} = T_{23} = v_3 = 0, \qquad Q_3 = 0 \qquad \text{on } X_3 = 0.02H \tag{2e}$$

$$T_{13} = T_{23} = T_{33} = 0, \qquad Q_3 = 0 \qquad \text{on } X_3 = 0.04H \tag{2f}$$

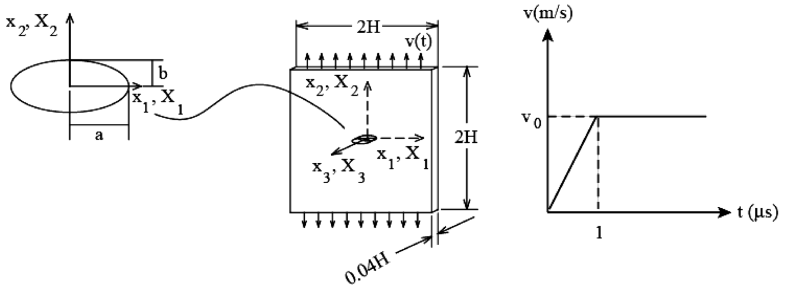

Fig. 1 Schematic sketch of the problem studied.

$$T_{\alpha\beta}N_\beta = 0, \quad Q_\alpha N_\alpha \qquad \text{on } \frac{X_1^2}{a^2} + \frac{X_2^2}{b^2} = 1, \qquad (\alpha, \beta = 1, 2) \tag{2g}$$

Here, **T** is the first Piola–Kirchhoff stress tensor, **Q** the heat flux per unit area in the reference configuration, **N** an outward unit normal to the surface of the elliptic void, and $2a$ and $2b$ are the major and minor axes of the elliptic void. Results are computed for different values of a and b with the axial velocity on the smooth top and the smooth bottom surfaces always applied along the X_2 axis. For $a \gg b$ and the major axis of the void along the X_1 axis, the state of deformation corresponds to mode 1.

Results have been computed only for the void opening mode, i.e., vertically upward velocity prescribed on the plate's top surface. Overall compressive deformations of the plate may collapse a void, necessitating the use of a contact algorithm to prevent interpenetration of nodes on one surface into the other contacting surface.

B. ASB and Crack Initiation Criteria

We assume that an ASB initiates at a point when the effective plastic strain there equals one and the material point is deforming plastically, and a crack ensues when the damage parameter D, given by

$$D = \sum \frac{\Delta\varepsilon^p}{\varepsilon_f}$$
$$\varepsilon_f = \left[D_1 + D_2 \exp\left(D_3\sigma^*\right)\right]\left[1 + D_4\, \ell n(\dot{\varepsilon}^*)\right]\left(1 + D_5 T^*\right) \tag{3}$$

equals one. In Eq. (3), the summation is performed over all time steps until the present time, $\Delta\varepsilon^p$ is the increment in the effective plastic strain during the incremental time Δt, $\dot{\varepsilon}^* = \dot{\varepsilon}^p/\dot{\varepsilon}_0$, $\sigma^* = \mathrm{tr}(\boldsymbol{\sigma})/\sigma_y$, $\boldsymbol{\sigma}$ is the Cauchy stress tensor, and constants D_1, D_2, D_3, D_4, and D_5 are material parameters. Thus, the present value of the damage D at a material point depends upon histories of the stress triaxiality ratio, the effective plastic strain, and the temperature. Hereafter, an element with $D = 1$ at its centroid is called a failed element. All stresses in a failed element are set equal to zero and remain zero for the rest of the analysis. The value of one for D at the initiation of a crack is taken from Benson [23] who used it to analyze the formation of chips in 4340 steel; otherwise, for a given material, values of D_1 and D_2 can be scaled to achieve this. We are not aware of any local failure criterion based on fracture toughness, stress triaxiality, and the aspect ratio of the void, etc., that is applicable for high-strain-rate problems.

Based on numerical experiments involving simple shearing deformations of 12 materials, Batra and Kim [24] proposed the following ASB initiation criterion: an ASB initiates at a point when the shear stress there has dropped to 80% of its peak value at that point, and 1) the material point is deforming plastically, and 2) the material surrounding the point is deforming inhomogeneously. For a simple shearing problem, this criterion quantifies Marchand and Duffy's [25] experimental observation that the torque required to deform the specimen drops very rapidly when an ASB initiates. As made clear by the plots in Fig. 1 of Batra and Lear's [18] paper, the side condition of the material point deforming plastically rules out the initiation of an ASB during elastic unloading of the body point. The other side condition is necessitated by the fact that ASBs do not form during homogeneous deformations of a body. During homogeneous deformations of the 4340 steel plate at a nominal strain rate of 500/s, the effective stress drops to 80% of the peak value at $\varepsilon^p = 1$. This provides at least a partial justification for our choice of taking $\varepsilon^P = 1$ as the ASB initiation criterion. Experimentalists generally decipher the formation of an ASB through postmortem observations of specimens, and call regions of intense plastic deformation distinctly separated from less deformed surrounding regions as shear bands. Whereas posttest observations can be made at points interior to the body, in situ observations are made at points on the bounding surfaces of the body. Thus, for an ASB and/or a crack originating from a point within the body, one needs to be careful in comparing computed results with test findings and ensure that deviations in quantities at the same point are being computed.

It is possible that under certain configurations of the void, a crack may precede an ASB even though it did not occur in any of our simulations. We note that values of material parameters at peak strain rates (nearly 10^5/s) and temperatures (close to half the melting temperature) likely to occur in the present problem are not available; they are assumed to be independent of temperature. Our goal is to see how the initiations of ASBs and cracks interact with each other.

A limitation of Eqs. (1) and (3) is that the flow stress does not depend upon the damage, and the damage cannot be easily correlated with the nucleation, coalescence, and growth of voids. A possibility is to postulate that the material is microporous with porosity distributed throughout the specimen. Chu and Needleman [26], amongst others, have used Gurson's [11] flow potential and considered the nucleation of voids in the evolution equation for the porosity. There are several material parameters in these constitutive relations whose values cannot be easily determined from the experimental data. As pointed out by Batra and Kim [6], values of material parameters determined by matching solutions of initial boundary-value problems with test observations are not necessarily unique because different sets of values of material parameters usually give the same final result. Even for a neo-Hookean (elastic) material, linear relations between different measures of stress and the corresponding strain tensors that give the same stress–strain curves for infinitesimal deformation yield quite different stress–strain curves for finite simple shear and simple extensional deformations, e.g., see Batra [27].

We note that concepts of fracture toughness and/or the J integral cannot be used to characterize the initiation and/or propagation of either an ASB or a crack in transient problems for thermo-elastoviscoplastic materials.

Wei and Batra [28] have recently deduced an evolution equation for damage in anisotropic rigid thermoviscoplastic materials. However, they neglected the effect of the nucleation of new voids and the coalescence of existing voids. Batra and Lear [18] modified slightly the porosity evolution equation used by Chu and Needleman [27] by requiring that the rate of porosity evolution be positive at a material point only when the mean stress there is tensile. Note that Eq. (3) implies that D can change even if $\sigma^* < 0$ because a material point can deform plastically under a negative mean stress. During elastic unloading characterized by $\Delta\varepsilon^P = 0$, D stays constant.

C. Simulation of Crack Propagation

To find the crack path, we locate, after every time step, centroids of failed elements. At the initiation of failure, the crack tip is located at the centroid of the failed element that is farthest from the origin or equivalently the center of the void. Subsequently, the crack tip is assumed to be at the centroid of the failed element that is farthest from the immediately preceding location of the crack tip, provided, of course, that all intermediate elements have also failed. Thus, the crack width is at least an element thick, and sharp cracks and/or those involving sliding of one surface over another are not considered. However, after a crack has initiated, subsequent non-interpenetration of points of one crack surface into the other crack surface is enforced by the penalty method. Note that the crack initiation criterion is local and does not involve a length scale. Furthermore, because of its dependence upon the histories of the triaxiality factor, the effective plastic strain, and the effective plastic strain rate, it simulates ductile failure rather than the brittle failure.

III. Computation and Discussion of Results

We used the computer code DYNA3D [29] to find an approximate solution of the aforementioned initial boundary-value problem, and assigned the following values to material (4340 steel) and geometric parameters:

$$\rho_0 = 7840 \text{ kg/m}^3, \quad \mu = 81 \text{ GPa}, \quad K = 161.2 \text{ GPa}$$
$$c = 477 \text{ J/kg} \cdot \text{K}, \quad A = 792 \text{ MPa}, \quad B = 510 \text{ MPa}$$
$$n = 0.26, \quad C = 0.014, \quad m = 1.03, \quad T_m = 1793 \text{ K}$$
$$T_a = 298 \text{ K}, \quad \dot{\varepsilon}_0 = 1/\text{s}, \quad D_1 = 0.05, \quad D_2 = 3.44$$
$$D_3 = -2.122, \quad D_4 = 0.002, \quad D_5 = 0.61$$
$$R = 0.125, 0.25, 1, 4, 8, \quad H = 1 \text{ mm}$$

Here ρ_0 is the initial mass density, μ the shear modulus, K the bulk modulus, $R = b/a$, and $2a$ and $2b$ equal, respectively, lengths of axes of the elliptic void along the X_1 and the X_2 axes. Values of material parameters in the Johnson–Cook relation (1) and the damage relation (3) for the 4340 steel are taken from Benson [23] who used them to study chip formation during the machining process.

The computer code DYNA3D uses the eight-node brick element, one-point integration rule to evaluate domain integrals, the lumped mass matrix, an hourglass control algorithm to eliminate spurious modes of deformation, and the explicit and conditionally stable central-difference method to integrate with respect to time the coupled nonlinear ordinary differential equations. During a time step, all deformations are presumed to be elastic and if the resulting stress state lies outside the current yield surface, the radial return algorithm is used to diminish stresses to lie on the yield surface. In the absence of heat conduction, the incremental temperature rise can be directly computed from the incremental plastic work done in a time step. In none of our computations did the temperature reach the melting point of the material.

The plate half-thickness is divided into five uniform layers, and discretizations of the plane $X_3 =$ constant for $R = 1$ and $R \neq 1$ are shown in Figs. 2a and 2b. A fine mesh close to the void enabled us to capture reasonably well intense plastic deformations in that region. The meshes of Figs. 2a and 2b gave virtually identical results for the plate with the circular void, suggesting that the irregular elements used to join the two sets of nearly uniform elements did not introduce any discernible errors. Four nodes on a face of the eight-node cubic master element are mapped onto a three-node triangle by mapping two nodes on a side of the four-node element onto the same node of the triangular element. The Jacobian of the transformation from the master element onto the actual element will vanish at the node onto which two nodes of the master element are mapped. However, DYNA3D uses the one-point integration rule with the element centroid taken as the integration point. Thus, nodal forces computed from the element stresses are reasonably accurate. These irregular elements can also influence the reflection and the transmission of waves at the boundaries between the two zones meshed with regular elements. Because an ASB and a crack ensue at large values of the effective plastic strain, errors introduced by the dispersion of mostly elastic waves at the interface between the two regions are minuscule as evidenced by the close agreement between the two sets of results for a circular void. For $R = 1/8$, $1/4$, 1, 4, and 8, the total number of elements (nodes) equaled 50,205 (56,359), 23,170 (26,290), 19,800 (22,550), 23,250 (26,400), and 52,000 (56,353), respectively. For each value of R, the principal axes of the ellipse coincide with the X_1 and the X_2 axes and the major axis of the elliptic void measured 0.08 mm. Thus, for $R = 1/8$ and $1/4$, the major axis of the elliptic void is aligned with the X_1 axis, and for $R = 4$ and 8 with the X_2 axis. Ideally, one should keep refining the mesh until a fully converged solution has been obtained. However, for a three-dimensional problem, this task is arduous and has not been attempted here. Our previous experience with the analysis of two-dimensional problems (e.g., see Table 1 in Batra and Lear [18]) has been that the computed ASB initiation times are fairly accurate when a reasonably fine mesh such as the one exhibited in Fig. 2 is employed. In the absence of heat conduction, the bandwidth cannot be determined and no attempt is made here to find it.

For plane-strain deformations of a heat-conducting thermoelastoviscoplastic solid, Batra and Love [19] analyzed the initiation and propagation of an ASB and a crack but they assumed that *either* an ASB *or* a crack initiated. Here, locally adiabatic three-dimensional deformations of a thermoelastoviscoplastic body are analyzed and the possibility of both a crack and an ASB initiating simultaneously and/or sequentially is allowed.

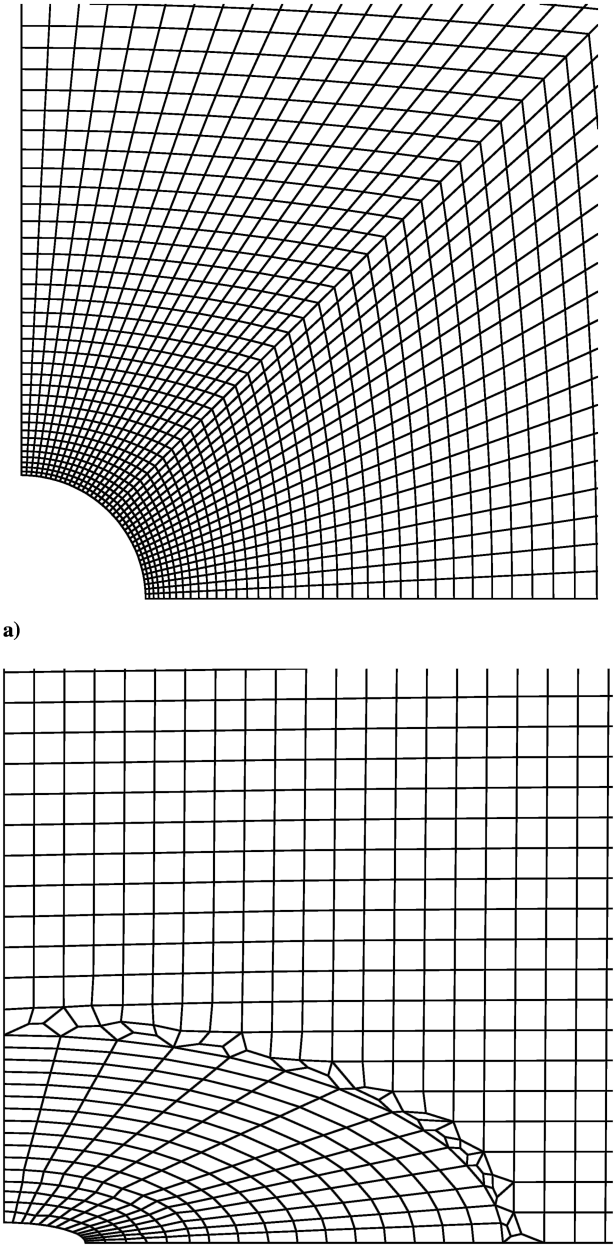

Fig. 2 Finite element discretization of a face of the plate for a) $R = 1$ (circular void), and b) $R = 0.25$ (elliptic void).

A. Results for a Circular Cylindrical Void

We first present and discuss results for $R = 1$, i.e., a circular void. To decipher where ASBs form and their directions of propagation, we have plotted in Fig. 3a evolution of the effective plastic strain ε_e^p at seven points, 1 (0.04, 0, 0.04), 2 (0.039, 0.009, 0.04), 3 (0.035, 0.019, 0.04), 4 (0.0282, 0.0282, 0.04), 5 (0.0195, 0.035, 0.04), 6 (0.009, 0.039, 0.04), 7 (0, 0.04, 0.04), on the void surface that are also on the front face of the plate. Point 1 is on the plane $X_2 = 0$, point 7 on the plane $X_1 = 0$, and point 4 on the plane $X_1 = X_2$. Time histories of ε_e^p at the corresponding points 15–21 on the plate's midsurface are exhibited in Fig. 3b. These results indicate that an ASB initiates first at $t \approx 32$ μs from point 15 located on the midsurface of the plate. By looking at the ASB initiation times at different points, we conclude

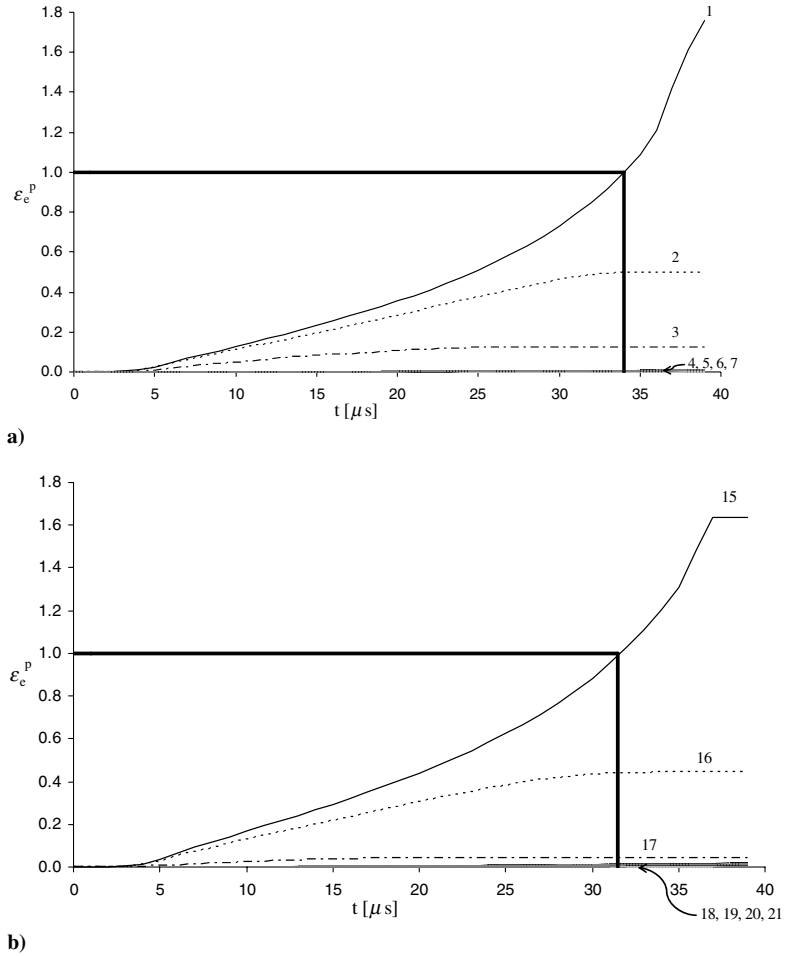

Fig. 3 Time histories of evolution of ε_e^p at a) points 1–7 on surface of circular void, also on front surface of plate, and b) points 15–21 on surface of circular void, also on midsurface of plate.

that it propagates in the thickness direction faster than it propagates along the X_1 axis. The effective plastic strain at point 15 appears steady for $t \geq 36$ μs because the material there failed at $t \approx 36$ μs; it is an artifact of plotting results rather than the actual effective plastic strain remaining unchanged because after failure, a material point cannot sustain any load and, hence, any deformation.

Figure 4 depicts at $t = 32$ μs fringe plots of the effective plastic strain on the front surface $X_3 = 0.04$ mm and a small region of the plane $X_2 = 0$ near the plate centroid. It is evident that the effective plastic strain is very large at points on the front surface of the plate that are on the line inclined at approximately 45 deg to the horizontal axis. The plot of Fig. 4b reveals the tunneling effect, i.e., ε_e^p is much larger in the central portion than that near the front and the back faces of the plate. One can also see the extent of the shear banded region, and notice that the thickness of the shear banded material along the X_1 axis is smaller than that of the material in the X_3 direction. Thus, the ASB propagates faster in the thickness direction than along the X_1 direction.

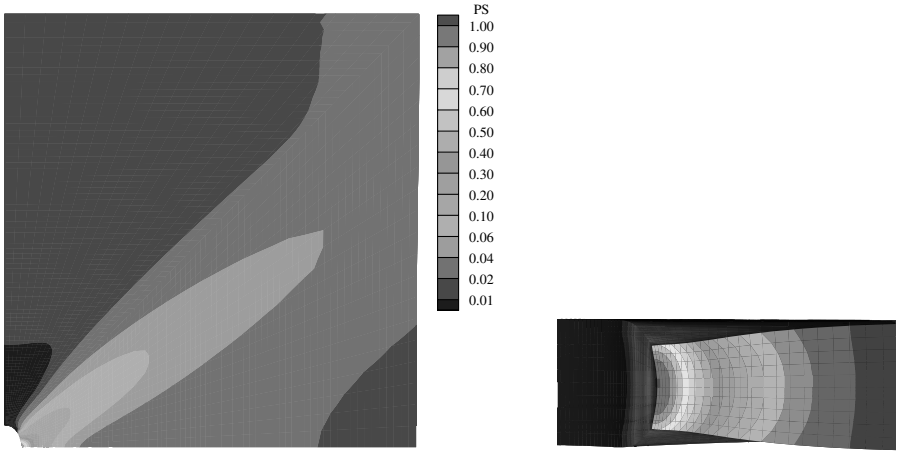

Fig. 4 Contours of the effective plastic strain at 32 μs on a) the front surface $X_3 = 0.04$ mm, and b) a small region near the plate centroid of the plane $X_2 = 0$.

To determine when and where a crack initiates, we have plotted in Fig. 5 the time history of the damage parameter D and the triaxiality factor σ^*. Recall that the damage D is given by Eq. (3) and the triaxiality factor affects how the damage evolves with time. We selected six points, 1 (0.0521,0,0.04), 2 (0.04,0,0.04), 3 (0.0392, 0.0078,0.04), 4 (0.0521,0,0.02), 5 (0.04,0,0.02), 6 (0.0392,0.0078, 0.02), close to the void tip; the last three of these points are on the midsurface of the plate and the first three are on the front surface. However, results for only points 1 and 4 are plotted here. Both points 1 and 4 are on the plane $X_2 = 0$, point 4 is on the midsurface of the plate and point 1 on the plate's front face. Upon arrival of the loading wave at points 1 and 4, the triaxiality factor rapidly increases to $\sim$1.3 and then gradually keeps increasing until the material point fails. The damage parameter rises monotonically from zero to its ultimate value of one; the rate of increase of D monotonically increases as the plate continues to be pulled at a uniform nominal axial strain rate. Note that deformations of the plate are inhomogeneous and the effective plastic strain is different at different points of the plate. The damage parameter D equals 1.0 at point 4 at $t = 35$ μs; subsequently, both D and the triaxiality factor drop to zero because the element has failed. Stresses in a failed element are set equal to zero. Whereas the material at point 4 has not failed until $t = 35$ μs, that at point 1 has not failed until $t = 38$ μs. When the material at point 4 fails at $t = 35$ μs, both the damage and the triaxiality factors at point 1 begin to increase more rapidly than that before the failure of the material at point 4. Upon failure of the material at point 4, the deletion of failed elements causes the plate to become 20% thinner locally along the X_3 axis passing through point 4, resulting in an increase in stresses in that region.

We note that an ASB initiates at a point on the midsurface of the plate at $t = 32$ μs and a crack at $t = 35$ μs. Thus, the crack follows the ASB as is believed to be the case in experiments.

B. Effect of Aspect Ratio or Void Shape on ASB/Crack Initiation Times

Table 1 summarizes the ASB/crack initiation times, and the initial crack speed for five values of R, namely 1/8, 1/4, 1, 4, and 8. Note that for $R = 1/8$, the major axis of the elliptic void is along the X_1 axis, i.e., perpendicular to the direction of the applied axial velocity, and the void is nearly a sharp crack; the state of deformation in this configuration is usually referred to as mode 1. For $R = 8$, the major axis of the elliptic void coincides with the direction of the applied velocity, i.e., the X_2 axis. The loading wave reaches the plate material on the X_3 axis at about 0.02 μs. It is clear that the ASB/crack initiation is considerably delayed for an elliptic void with the major axis parallel to the direction of loading as compared with that of the major axis perpendicular to the direction of loading. Whereas, for $R = 1/4$ and 1/8, the ASB and the crack initiate simultaneously (within the time interval of the output); for $R = 1$, 4, 8 the crack initiates later than the ASB does. Also, the initiation of the ASB and the crack is delayed with an increase in the value of R.

Table 1 For different values of R, initiation times of an ASB, and a crack at a point on plate's midsurface that is also on the void surface, and initial crack speeds

R	t_{ASB}, μs	t_{crack}, μs	Initial crack Speed, m/s
8	137	142	19.75
4	86	93	19.11
1	32	35	34.61
0.25	15	15	29.53
0.125	7	7	22.93

For $R = 1/8$, Figs. 6a and 6b exhibit the crack path as seen from the X_3 axis and also its path in the three-dimensional space. Numbers in the three-dimensional plot indicate time in microseconds subsequent to the initiation of the crack. It is clear that the crack tip follows a zigzag path that does not lie in one plane. Batra and

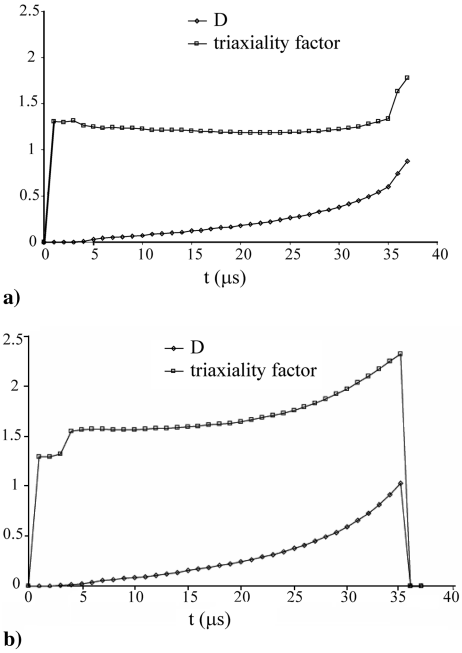

Fig. 5 Time histories of damage parameter D and the triaxiality factor $(\sigma_{11} + \sigma_{22} + \sigma_{33})/\sigma_y$ at two points: a) point 1 on the front face, and b) point 4 on the midsurface.

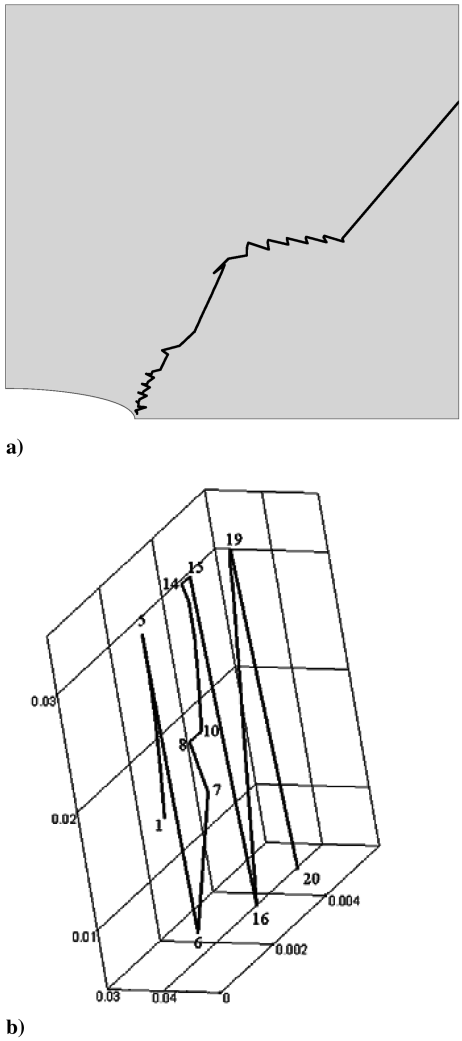

Fig. 6 For $R = 1/8$, crack paths a) as seen from the X_3 axis, and b) the three-dimensional view (numbers indicate time in μs, subsequent to crack initiation).

Ravisankar [13] analyzed ASB initiation in a prenotched plate, impacted on the notched side by a cylindrical projectile, and found that the ASB tip also followed a zigzag path; cf. Fig. 8 of their paper. These studies suggest that, at least in a rectangular plate, the shear banded region is not simply connected, and its shape does not resemble a disk with periphery expanding outwards. The initial crack speed computed from the distance between two consecutive locations of the crack tip and the elapsed time is also listed in Table 1. Even though the initial crack speed does not strongly depend upon R, the final crack speed and the resulting deformed shape vary rather noticeably with R. For the first 20 μs after initiation, the crack stays confined to the region $(0, 0.005) \times (0, 0.03) \times (0, 0.03)$ mm; here, the midsurface is denoted by $X_3 = 0$.

Simulations were stopped at $t = 200$ μs; at that instant, the crack was longer for smaller values of R. For $R = 1/8$ and $1/4$, the deformed plate was separated into two parts but for R = 1, 4, and 8, the plate stayed in one piece; cf. Fig. 7. It is interesting to observe from Fig. 7b that a significant portion of the plate material adjacent to the X_2 axis has failed and a narrow region of low effective stress, usually associated with an ASB, has developed. The effective plastic strain in this narrow region was found to be high, thereby confirming the localization of deformation in it. This is an example of the formation of an ASB that resulted in the failure of the plate material and another ASB originating from a boundary of the cracked or failed region, and has been computed for the first time.

To ascertain the order of singularity for $R = 1$, we plotted on a log–log plot at $t = 10$ and 30 μs the variation of the effective plastic strain vs the distance, from the void tip, of points on the midsurface of the plate along the X_1 axis. Slopes of least-squares fit straight lines equaled, respectively, -2.67 and -2.96 at $t = 10$ and $t = 30$ μs. Thus, the order of singularity changes a little with time. Note that for $R = 1/8$, an ASB and a crack initiated at $t \approx 7$ μs and, consequently, the order of singularity at the void tip was not computed.

C. Effect of Plate Thickness

For a nominal strain rate of 1000/s and a circular cylindrical void (i.e., $R = 1$), Table 2 lists the ASB and the crack initiation times for three values of the plate thickness. Both times increase with an increase in the plate thickness. For the 0.004-mm-thick plate, one-half of the plate thickness was divided into two uniform layers. For the smallest thickness of the plate, a crack initiated before the initiation of an ASB. Results were also computed by constraining displacements of all nodes in the thickness direction to be zero; these are referred to as two-dimensional rather than plane strain in Table 2 because there is no guarantee that u_1 and u_2 are independent of the thickness coordinate. For the two-dimensional analysis, both the ASB and the crack initiation times fall between those for plates with thicknesses of 0.04 and 0.4 mm. Because we did not analyze three-dimensional deformations of plates of other thicknesses, we cannot draw definite conclusions. However, one can conclude that the ASB/crack initiation times computed from the two-dimensional analysis are not representative of those from the three-dimensional analysis. In this regard, we add that for a prenotched plate impacted on the notched side, the two-dimensional and the three-dimensional analyses [14] gave ASB initiation times of 15.2 and 23.84 μs, respectively. For the same problem, Batra and Ravisankar [13] used DYNA3D and found ASB initiation times to be 15.8 and 24 μs for the two-dimensional and the three-dimensional analyses. Whereas Batra and Wang [14] accounted for heat conduction and porosity evolution, Batra and Ravisankar [13] neglected these effects.

Table 2 For $R = 1$, effect of the plate thickness on ASB and crack initiation times

Plate thickness, mm	t_{ASB}, μs	t_{crack}, μs
0.004	——	23
0.04	32	35
0.4	89	97
2D	59	61

D. Remarks

A shortcoming of the present work is the deletion from the analysis of failed elements, thereby making the crack dimensions equal to the size of the failed element. For plane-strain problems, the nodal release technique has been employed to simulate crack initiation and propagation by using four-node quadrilateral [19] and three-node triangular [30] elements, respectively. The crack was allowed to propagate along the boundary between two adjoining elements and thus its elongation at a given time equaled the distance between adjoining nodes. The simulated brittle failure assumed that a crack initiates at a node when the maximum principal tensile stress there reaches a critical value. In a prenotched plate, impact loaded on the notched side by a cylindrical projectile, it was found that the initiation of a brittle crack delayed the initiation of an ASB. Batra and Love [19] also studied the initiation of a ductile crack in a heat-conducting thermoelastoviscoplastic plate undergoing plane-strain simple shearing deformations. They assumed that a ductile crack initiates when the effective plastic strain reaches a critical value and the newly formed crack surfaces are thermally insulated and smooth. Because of the loading conditions, the crack did not open and the two newly formed crack surfaces slid over each other.

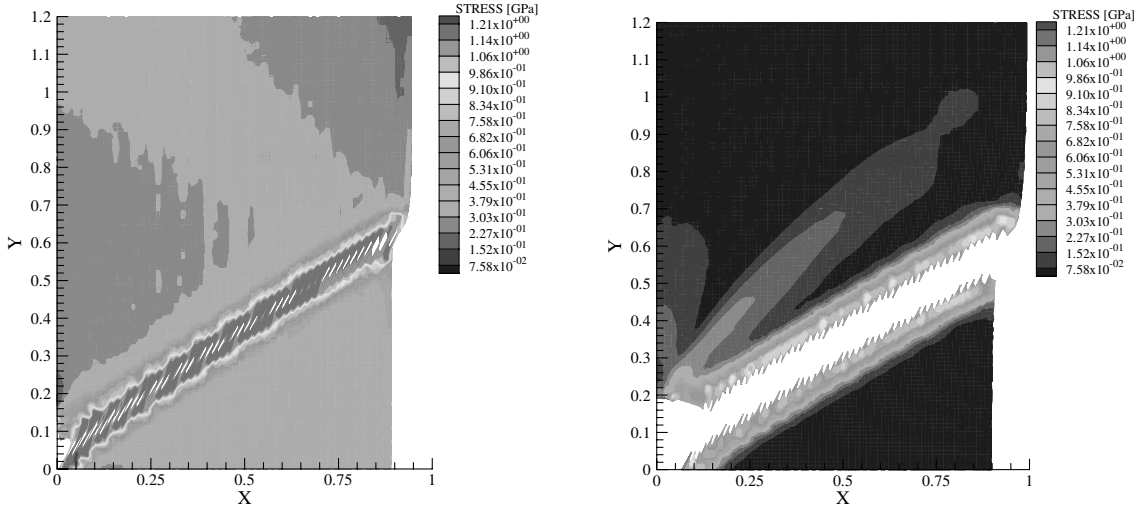

a) b)

Fig. 7 Contours of effective stress in the deformed plate at $t = 200$ μs for a) $R = 8$, and b) $R = 1/8$.

For one- and two-dimensional transient thermomechanical problems, the effect of different material parameters on the ASB initiation time has been delineated [31,32]. Batra and Gummalla [32] used DYNA2D to study the shear banding in a prenotched SAE 4340 steel plate impacted on the notched side. Results plotted in Fig. 9 of their paper imply that for the Johnson–Cook constitutive relation (1), material parameters A, B, T_m, and m, the plate thickness, and the geometric parameter r_0 that equaled the notch-tip radius strongly influenced the ASB time. The analogue of r_0 for the present problem is R. Thus, the aspect ratio R of the elliptic void, and the quasi-static yield stress A, the strain-hardening parameter B, and parameters T_m and m characterizing the thermal softening of the material, need to be more precisely determined than other material parameters.

We have considered only one void in the homogeneous plate. However, in practice, voids of different shapes, orientations, and sizes are likely to be distributed throughout the body. A possibility is to simulate these by postulating the material to be microporous and employ Gurson's [11] flow potential or one of its modifications.

The initiation and development of ASBs and fracture in a heterogeneous body are more involved than those in a homogeneous body. Batra and Love [33] have analyzed ASBs in a particulate composite deformed at high strain rates in plane-strain tension/compression and found that an ASB initiation criterion suitable for a homogeneous body needs to be modified for a heterogeneous body. They proposed that an ASB initiates at a material point when the energy dissipation rate there increases essentially by an order of magnitude. For a homogenous body, this criterion gives the same results as that employed here.

IV. Conclusions

We have studied numerically with the finite element method, transient locally adiabatic thermomechanical deformations of a rectangular plate with a through-the-thickness centroidal void and deformed in simple tension. Both an adiabatic shear band and a crack are allowed to initiate at a point. It is found that their initiation strongly depends upon the void shape and the plate thickness. Their initiation times increase with an increase in the plate thickness, and also with an increase in the ratio $R = b/a$, where $2a$ and $2b$ equal, respectively, lengths of the axes of the elliptic void along the X_1 and the X_2 axes with the axial velocity applied along the X_2 axis. For a square plate of thickness/height $= 0.02$ and $R = 1/4$ and $1/8$, a crack and an adiabatic shear band initiate simultaneously, whereas for $R = 1$, 4, and 8, the shear band initiates first. For $R = 1/8$, the plate was separated into two pieces, and an adiabatic shear band also originated from a point on the void surface that is close to the plane $X_1 = 0$. The adiabatic shear band and the crack initiation times from the two-dimensional analysis differ noticeably from those computed with the three-dimensional analysis. The crack tip and the adiabatic shear band tip follow a zigzag path that does not lie in one plane, and the shear banded region does not appear to be simply connected in the form of a disk whose periphery expands outwards along the normal to the boundary.

Acknowledgments

This work was partially supported by the Office of Naval Research grants N00014-98-1-0300 and N00014-06-1-0576 to Virginia Polytechnic Institute and State University with Y. D. S. Rajapakse as the program manager. Views expressed herein are those of the authors, and neither of the funding agency nor of Virginia Polytechnic Institute and State University.

References

[1] Tresca, H., "On Further Application of the Flow of Solids," *Proceedings of the Institution of Mechanical Engineers*, Vol. 30, 1878, pp. 301–345.

[2] Massey, H. F., "Flow of Metal During Forging," *Proceedings of the Manchester Association of Engineers*, 1928, pp. 21–26.

[3] Zener, C., and Hollomon, J. H., "Effect of Strain Rate upon Plastic Flow of Steel," *Journal of Applied Physics*, Vol. 15, No. 1, 1944, 22–32.

[4] Clifton. R. J., "Adiabatic Shear in Material Response to Ultrahigh Loading Rates," edited by Herrmann, W., National Research Council National Material Advisory Board (U.S.) Rept. NMAB-36, Washington, DC, 1980.

[5] Bai, Y. L., "Thermoplastic Instability in Simple Shear," *Journal of the Mechanics and Physics of Solids*, Vol. 30, No. 4, 1982, pp. 195–207.

[6] Batra, R. C., and Kim, K. H., "Effect of Viscoplastic Flow Rules on the Initiation and Growth of Shear Bands at High Strain Rates," *Journal of the Mechanics and Physics of Solids*, Vol. 38, No. 6, 1990, pp. 859–874.

[7] Batra, R. C., and Kim, C. H., "Adiabatic Shear Banding in Elastic-Viscoplastic Nonpolar and Dipolar Materials," *International Journal of Plasticity*, Vol. 6, No. 2, 1990, pp. 127–141.

[8] Bai, Y. L., and Dodd, B., *Adiabatic Shear Localization: Occurrence, Theories, and Applications*, Pergamon, Oxford, England, UK, 1992.

[9] Wright, T. W., *Physics and Mathematics of Adiabatic Shear Bands*, Cambridge Univ. Press., Cambridge, England, UK, 2002.

[10] Bronkhorst, C. A., Cerreta, E. K., Xue, Q., Maudlin, P. J., Mason, T. A., and Gray, G. T., "Experimental and Numerical Study of the Localization Behavior of Tantalum and Stainless Steel," *International Journal of Plasticity*, Vol. 22, No. 7, 2006, pp. 1304–1335.

[11] Gurson, A. L., "Continuum Theory of Ductile Rupture by Void Nucleation and Growth: Part 1," *Journal of Engineering Materials and Technology*, Vol. 99, No. 1, 1977, pp. 2–15.

[12] Batra, R. C., and Ko, K. I., "Analysis of Shear Bands in Dynamic Axisymmetric Compression of a Thermoviscoplastic Cylinder," *International Journal of Engineering Science*, Vol. 31, No. 4, 1993, pp. 529–547.

[13] Batra, R. C., and Ravisankar, M. V. S., "Three-Dimensional Numerical Simulation of the Kalthoff Experiment," *International Journal of Fracture*, Vol. 105, No. 2, 2000, pp. 161–186.

[14] Batra, R. C., and Wang, Z., "Failure Mode Transition Speed in Three-Dimensional Transient Deformations of a Microporous Heat-Conducting Thermoelastoviscoplastic Pre-Notched Plate," *Journal of Thermal Stresses*, Vol. 28, No. 5, 2005, pp. 533–562.

[15] Zabib, H. M., and Jubran, J. S., "Dynamic Shear Banding: aThree-Dimensional Analysis," *International Journal of Plasticity*, Vol. 8, No. 6, 1992, pp. 619–641.

[16] Batra, R. C., and Zhang, X., "On the Propagation of a Shear Band in a Steel Tube," *Journal of Engineering Materials and Technology*, Vol. 116, No. 2, 1994, pp. 155–161.

[17] Batra, R. C., and Kim, C. H., "Effect of Thermal Conductivity on the Initiation, Growth and Band Width of Adiabatic Shear Bands," *International Journal of Engineering Science*, Vol. 29, No. 8, 1991, pp. 949–960.

[18] Batra, R. C., and Lear, M. H., "Adiabatic Shear Banding in Plane Strain Tensile Deformations of 11 Thermoelastoviscoplastic Materials with Finite Thermal Wave Speed," *International Journal of Plasticity*, Vol. 21, No. 8, 2005, pp. 1521–1545.

[19] Batra, R. C., and Love, B. M., "Crack Propagation Due to Brittle and Ductile Failures in Microporous Thermoelastoviscoplastic Functionally Graded Materials," *Engineering Fracture Mechanics*, Vol. 72, No. 12, 2005, pp. 1954–1979.

[20] Johnson, G. R., and Cook, W. H., "Constitutive Model and Data for Metals Subjected to Large Strains, High Strain Rates, and High Temperatures," *Proceedings of the 7th International Symposium on Ballistics*, The Hague, The Netherlands, 1983, pp. 541–548.

[21] Truesdell, C. A., and Noll, W., *Nonlinear Field Theories of Mechanics*, edited by S. Flügge, Handbuch der Physik, Vol. 3, Springer, Berlin, 1965.

[22] Batra, R. C., *Elements of Continuum Mechanics*, AIAA, Reston, Virginia, 2005.

[23] Benson, D. J., "Mixture Theory for Contact in Multi-Material Eulerian Formulations," *Computer Methods in Applied Mechanics and Engineering*, Vol. 140, Nos. 1–2, 1997, pp. 59–86.

[24] Batra, R. C., and Kim, C. H., "Analysis of Shear Bands in Twelve Materials," *International Journal of Plasticity*, Vol. 8, No. 4, 1992, pp. 425–452.

[25] Marchand, A., and Duffy, J., "Experimental Study of the Formation of Adiabatic Shear Bands in a Structural Steel," *Journal of the Mechanics and Physics of Solids*, Vol. 36, No. 3, 1988, pp. 251–283.

[26] Chu, C. C., and Needleman, A., "Void Nucleation Effects in Bi-Axially Stretched Sheets," *Journal of Engineering Materials and Technology*, Vol. 102, No. 3, 1980, pp. 249–256.

[27] Batra, R. C., "Comparison of Results from Four Linear Constitutive Relations in Isotropic Finite Elasticity," *International Journal of Non-Linear Mechanics*, Vol. 36, No. 3, 2001, pp. 421–432.

[28] Wei, Z. G., and Batra, R. C., "Damage Model for Anisotropic Materials, and its Application to Analysis of Stability and Spallation," *International Journal of Impact Engineering*, 2007 (to be published).

[29] Whirley, R. G., and Hallquist, J. P., "DYNA3D User's Manual, a Nonlinear, Explicit, Three-Dimensional Finite Element Code for Solid and Structural Mechanics," Lawrence Livermore National Lab. Rept. UCRL-MA-107254, 1991.

[30] Batra, R. C., and Lear, M. H., "Simulation of Brittle and Ductile Fracture in an Impact Loaded Prenotched Plate," *International Journal of Fracture*, Vol. 126, No. 2, 2004, pp. 179–203.

[31] Batra, R. C., "Effect of Material Parameters on the Initiation and Growth of Adiabatic Shear Bands," *International Journal of Solids and Structures*, Vol. 23, No. 10, 1987, pp. 1435–1446.

[32] Batra, R. C., and Gummalla, R. R., "Effect of Material and Geometric Parameters on Deformations near the Notch-Tip of a Dynamically Loaded Prenotched Plate," *International Journal of Fracture*, Vol. 101, Nos. 1–2, 2000, pp. 99–140.

[33] Batra, R. C., and Love, B. M., "Mesoscale Analysis of Shear Bands in High Strain Rate Deformations of Tungsten/Nickel-Iron Composites," *Journal of Thermal Stresses*, Vol. 28, Nos. 6–7, 2005, pp. 747–782.

A. Roy
Associate Editor